

Real-time Forecasting of Dockless Scooter-Sharing Demand: A Context-Aware Spatio-Temporal Multi-Graph Convolutional Network Approach

Yiming Xu^a, Mudit Paliwal^b, Xilei Zhao^{a,*}

^a*Department of Civil and Coastal Engineering, University of Florida, Gainesville, FL*

^b*Department of Industrial and Systems Engineering, University of Florida, Gainesville, FL*

Abstract

Real-time demand forecasting for shared micromobility can greatly enhance its potential benefits and mitigate its adverse effects on urban mobility. The deep learning models provide researchers powerful tools to deal with the real-time dockless scooter-sharing demand prediction problem, but existing studies have not fully incorporated the features that are highly associated with the demand, such as weather conditions, demographic characteristics, and transportation supply. This paper proposes a novel deep learning model named Context-Aware Spatio-Temporal Multi-Graph Convolutional Network (CA-STMGCN) to forecast the real-time spatiotemporal dockless scooter-sharing demand. The proposed model applies a graph convolutional network (GCN) component that uses spatial adjacency graph, functional similarity graph, demographic similarity graph, and transportation supply similarity graph as input to extract spatial dependency and attach it to historical demand data. Then, we use a gated recurrent unit component to process the output of GCN and weather condition data to capture temporal dependency. A fully connected neural network layer is used to generate the final prediction. The proposed model is evaluated using the real-world dockless scooter-sharing demand data in Washington, D.C. The results show that CA-STMGCN significantly outperforms all the selected benchmark models, and the most important model component is the weather information. The proposed model can help the operators develop optimal vehicle rebalancing schemes and guide cities to regulate the dockless scooter-sharing usage.

Keywords: Dockless scooter-sharing, Deep learning, Demand forecasting, Shared micromobility

1. Introduction

Shared micromobility refers to small, single-passenger transportation modes rented for short-term use, such as dockless bike-sharing and scooter-sharing. Shared micromobility is

*Corresponding author. Address: 1949 Stadium Rd, Gainesville, FL 32611. Phone: +01 352-294-7159. Email: xilei.zhao@essie.ufl.edu.

flexible, convenient, affordable, environmentally friendly, and fun to use, making it especially attractive to serve short-distance trips and offer a potential solution to the “first mile/last mile” problem that has long troubled public transit. Among all the shared micromobility options, dockless scooter-sharing are growing at the fastest pace (NACTO, 2019). In 2019, people in the U.S. took 86 million trips on dockless scooter-sharing systems, contributing to an over 100% increase from 2018 (NACTO, 2019).

While dockless scooter-sharing as a travel mode can greatly enhance urban mobility, it is faced with two major operation challenges. Firstly, the trip origin and destination demands of dockless scooter-sharing are unbalanced spatially and temporally (McKenzie, 2019; Merlin et al., 2021; Xu et al., 2020). For example, the spatial distribution of commuter trip origins and destinations are significantly unbalanced during the morning peak and the afternoon peak. The commuter trip origin demand in residential areas is high during the morning peak but low during the afternoon peak, while that demand in commercial areas is low during the morning peak but high during the afternoon peak (Xu et al., 2020). Since many places have limited parking space for scooters, unbalanced trip demand may lead to a large number of scooters gathering in some places and spilling out of the parking spaces, thus inhibiting other activities and causing safety issues. The gathering of scooters needs to be anticipated to ensure that the redundant scooters are removed in time to mitigate the adverse effects. In light of this, accurate spatiotemporal dockless scooter-sharing demand predictions are essential for generating optimal rebalancing strategies (Schuijbroek et al., 2017) and removing the redundant scooters. Secondly, the scooters need to be recharged when they are at a low power level. To accomplish this, the operators collect these low-power-level vehicles, recharge them, and then drop them off at specific locations. In this case, accurate dockless scooter-sharing demand predictions are needed to determine the optimal scooter drop-off locations.

Although some recent studies (e.g., Bai and Jiao (2020); McKenzie (2019); Zhu et al. (2020)) have examined the spatiotemporal patterns of dockless scooter-sharing in different cities, few studies shed lights on the highly-accurate real-time spatiotemporal dockless scooter-sharing demand prediction. Additionally, most real-time shared micromobility demand forecasting studies are focused on station-based (i.e., docked) bike-sharing (Chen et al., 2020; Li et al., 2019; Lin et al., 2018; Pan et al., 2019). Based on models such as recurrent neural network (RNN), convolutional neural network (CNN), and graph convolutional network (GCN), these studies abstracted the stations into nodes in a graph and assigned the demand to these nodes. Although these models achieved a decent prediction performance for station-based bike-sharing demand forecasting, applying these models to dockless scooter-sharing demand forecasting can be tricky since there are no parking stations for dockless scooter-sharing. The station-based bike-sharing trips can only take place at the stations while dockless scooter-sharing trips can happen at any places where no parking restrictions for e-scooters exist. Therefore, the origin and destination demand of station-based bike-sharing is concentrated in the stations while the spatial distribution of dockless scooter-sharing demand is more scattered. There is a pressing need to study spatiotemporal demand forecasting for dockless scooter-sharing services.

In this paper, we propose a novel deep learning model named *Context-Aware Spatio-*

Temporal Multi-Graph Convolutional Network (CA-STMGCN) to deal with the real-time dockless scooter-sharing demand forecasting problem. The proposed model can simultaneously capture spatial and temporal dependency and takes zonal context and weather conditions into account to achieve higher prediction performance. We first use four graphs to encode the spatial correlations (i.e., spatial adjacency, functional similarity, demographic similarity, and transportation supply similarity). After that, we use a GCN model to process these graphs to extract spatial dependency and attach the spatial dependency to the time series data (i.e., historical demand). Then, we use a GRU model to take the time series data with spatial dependency and weather condition data to capture temporal dependency. At last, a fully connected neural network layer is used to generate the final prediction. The contributions of this paper are twofold: (1) We propose a context-aware deep learning framework that captures spatial and temporal dependency simultaneously to forecast the real-time dockless scooter-sharing demand. The new model takes into account critical features about demographics, the zonal functionality, the transportation supply, and weather conditions; and (2) the proposed model significantly outperforms the state-of-the-art benchmark models, based on an real-world dockless scooter-sharing demand dataset collected from Washington, D.C.

The remainder of this paper is structured as follows. Section 2 reviews existing literature related to this study. Section 3 formally defines the research problem and describes the proposed method from the overall model architecture to its specific components. Section 4 presents a case study in Washington, D.C., and compares the performance of the proposed model with several benchmark models. Section 5 concludes the paper by summarizing findings, identifying limitations, and suggesting future work.

2. Literature Review

2.1. Travel Demand Forecasting Methods

The travel demand forecasting problem has been intensively studied by researchers in the past decades. Different forecasting models have been proposed and applied to this problem. These models can be roughly categorized into 3 categories: the statistical models, the machine learning models, and the deep learning models.

The historical average (HA) model and the auto-regressive integrated moving average (ARIMA) model are typical statistical models. They have been widely used in demand prediction problems. For example, Amini et al. (2016) presented a ARIMA based model to forecast the charging demand of electric vehicles. Smith et al. (2002) applied the ARIMA model in short-term traffic flow demand forecasting. Most of the statistical models are based on regressions and use the historical demand to do predictions.

The machine learning models for demand forecasting include random forest (RF), gradient boosting decision tree (GBDT), support vector regression (SVR), and so on. For example, Ashqar et al. (2021) used random forest and boosting to predict the number of available bikes at the station-level. Yan et al. (2020) developed a random forest model to predict the zone-to-zone (census tract) direct demand for ridesourcing services. These

models are classical machine model. The models can learn temporal dependency from the historical demand, but they cannot capture spatial dependency.

The deep learning methods have provided researchers powerful tools to deal with travel demand prediction problems, such as taxi demand prediction (Liu et al., 2019; Xu et al., 2017; Yao et al., 2018), ride-hailing demand prediction (Geng et al., 2019), ridesourcing demand prediction (Ke et al., 2021), and bike-sharing demand prediction (Kim et al., 2019; Li et al., 2019; Lin et al., 2018). Since the demand varies spatially and temporally, different deep learning methods were used to capture spatial dependency and temporal dependency in these studies, and the results showed that these deep learning methods outperformed the classical machine learning models (e.g., RF and GBDT) and the statistical models (e.g., linear regression and ARIMA). In these demand prediction tasks, the convolutional neural networks (CNNs) and graph convolutional networks (GCNs) are usually used to capture the spatial dependency, and the recurrent neural networks (RNNs) such as gated recurrent unit (GRU) and long short-term memory (LSTM) models are usually used to capture the temporal dependency (Chen et al., 2020; Pan et al., 2019). Some studies also combined these two kinds of neural networks into a spatiotemporal model to capture spatial and temporal dependency simultaneously, and the results showed that the spatiotemporal models have better performance than the single CNN or RNN models (Geng et al., 2019; Tang et al., 2021; Yao et al., 2018).

Given the effectiveness of deep learning methods on demand forecasting tasks, different kinds of deep learning models have been applied for shared micromobility demand prediction in previous studies, including the RNN models (Chen et al., 2020; Pan et al., 2019) and the spatiotemporal models (Lin et al., 2018; Liu et al., 2019). Although some of these models can capture spatial and temporal dependency, they only consider the geographical adjacency relationships between zones when extracting spatial dependency. Many spatial factors, such as the zonal functionality and demographic and built environment characteristics (e.g., population density) that are highly related to passenger trip demand (Bai and Jiao, 2020; Xu et al., 2021) are omitted in these models. In addition, the usage of shared micromobility is sensitive to weather conditions (Noland, 2021; Younes et al., 2020), but few existing spatiotemporal models took the weather conditions into account (e.g., Kim et al., 2019). To fill these gaps mentioned above, we take the weather conditions into account and construct several graphs to include more zonal characteristics in the model input to make the spatial information in our model more comprehensive.

2.2. Factors Associated with Dockless Scooter-Sharing Usage

Many factors have been examined by the researchers to understand the influence of these factors on dockless scooter-sharing usage. These factors can be categorized as weather conditions, demographic factors, built environment factors, and land use factors.

Literature showed that the weather conditions, such as temperature, precipitation, and wind speed, can greatly influence the usage of dockless scooters (Mathew et al., 2019; Noland, 2021; Younes et al., 2020). For example, the rainy and cold weather will significantly reduce the use of dockless scooter-sharing services (Noland, 2021).

The demographic factors include age, gender, income, education level, race, resident status, and so on. The literature suggested that the young people, the male, the people with high income, and highly educated people were more likely to use the dockless scooter-sharing services (Cao et al., 2021; Christoforou et al., 2021; Laa and Leth, 2020; Lee et al., 2021; Mitra and Hess, 2021; Sanders et al., 2020). Dockless scooter-sharing usage were also found to be positively associated with some zonal demographic characteristics including population density, employment rate, proportion of young population, and proportion of high educated population (Bai and Jiao, 2020; Caspi et al., 2020; Merlin et al., 2021).

The most significant built environment factor related to the usage of dockless scooter-sharing was the transportation supply factors, such as the quality of riding environment, especially the street safety (Hosseinzadeh et al., 2021; Mitra and Hess, 2021; Sanders et al., 2020), and access to transit stations. Areas with better riding environment (i.e., higher Walk Score and Bike Score, and better bicycle infrastructure) often had a high density of shared-scooter trips (Caspi et al., 2020; Hosseinzadeh et al., 2021). Areas with higher transit station density usually had more shared-scooter trips (Bai and Jiao, 2020; Merlin et al., 2021).

Land use factors were also associated with the spatial usage patterns of shared-scooters: greater land use diversity and higher proportion of commercial land use were positively correlated with shared-scooter demand (Bai and Jiao, 2020; Hosseinzadeh et al., 2021; Merlin et al., 2021).

Since the factors discussed above can greatly influence the usage of dockless scooter-sharing, these factors should be considered when forecasting the dockless scooter-sharing demand. Although some existing demand forecasting models has taken some of these factors into account (Ke et al., 2021; Tang et al., 2021), few studies comprehensively included all kinds of these factors in their models when predicting the real-time dockless scooter-sharing demand, especially the weather conditions.

3. Methodology

3.1. Research problem definition

In this section, we formally define the zonal dockless scooter-sharing demand prediction problem and introducing several key inputs used in our study.

Definition 1: Dockless scooter-sharing demand x_t^i . We first divide the study area into several zones. In previous studies on demand prediction (Geng et al., 2019; Liu et al., 2019; Yao et al., 2018), the study area was usually divided into regular cells (e.g., squares and hexagons). Although that kind of segmentation enables the use of standard machine learning algorithms (e.g., CNNs), it cannot well represent the functional and administrative properties of the zones (Ke et al., 2021). Therefore, in this study, we divide the study area by the census block groups, in which the socioeconomic and demographic properties are homogeneous. After that, we count the number of dockless scooter-sharing uses at the census block group level during a specific time interval. The aggregated result is defined as dockless scooter-sharing demand. The dockless scooter-sharing demand of the block group i at time interval t is denoted by x_t^i .

Definition 2: Node correlation graph G . We use an unweighted graph $G = (V, E)$ to describe the spatial and property correlation between the nodes (i.e., census block groups). This graph is fused by multiple graphs to represent the spatial adjacency relationship, functional similarity, demographic similarity, and transportation supply similarity between the zones. In graph $G = (V, E)$, as we treat each census block group as a node, $V = \{v_1, v_2, \dots, v_N\}$ is a set of census block groups, where N is the number of census block groups. E is a set of edges. If two nodes (i.e., census block groups) are correlated (e.g., spatially adjacent or have similar functionality), there is an edge between these two nodes. An adjacency matrix $A \in \mathbb{R}^{N \times N}$ can be used to represent the graph G . The element $a_{ij} \in A$ is 1 if there is an edge between node i and node j , otherwise, the element a_{ij} is 0. The details of node correlation modeling are discussed in Section 3.6.

Definition 3: Feature matrix $X^{N \times T}$. We use the dockless scooter-sharing demand as the features of the nodes. In feature matrix $X^{N \times T}$, N is the number of nodes (i.e., census block groups), and T is the number of node features (i.e., the length of input historical demand data). $X_t = [x_t^1, x_t^2, \dots, x_t^N]$ denote the dockless scooter-sharing demand of all census block groups at time t .

Definition 4: Weather condition matrix $C^{N \times M}$. The dockless scooter-sharing demand can be greatly influenced by the weather. We use a weather matrix $C^{N \times M}$ to represent the weather conditions of nodes, where N is the number of nodes and M is the number of weather features (e.g., temperature, precipitation, and wind speed).

The zonal dockless scooter-sharing demand prediction problem can be formulated as follows.

Problem: Given a node correlation graph G , a weather condition matrix C , and a feature matrix X , learn a function $f : \mathbb{R}^{N \times T} \rightarrow \mathbb{R}^N$ that maps historical dockless scooter-sharing demand of all zones to the dockless scooter-sharing demand in the next time interval:

$$X_{t+1} = f(G, C, [X_{t-T+1}, \dots, X_t]) \quad (1)$$

3.2. Overview of model framework

We propose a *Context-Aware Spatio-Temporal Multi-Graph Convolutional Network* (CA-STMGCN) model to solve the research problem. The model framework is presented in Figure 1. The proposed CA-STMGCN model consists of two modules: the graph convolutional network (GCN) to capture node correlation dependency and the gated recurrent unit (GRU) to capture temporal dependency. Specifically, we first construct four graphs to encode the spatial correlations (i.e., adjacency, functional similarity, demographic similarity, and transportation supply similarity) between the nodes. These multiple graphs are processed and fused by GCN to obtain node correlation dependency. After that, we combine the historical dockless scooter-sharing demand data with the extracted node correlation dependency and weather conditions. The combined data is taken as the input of the GRU layers to capture temporal dependency. Finally, the demand prediction is generated by the fully connected layer, and the model loss is evaluated using the labels. We introduce the detailed methods of different modules of the framework in the following subsections.

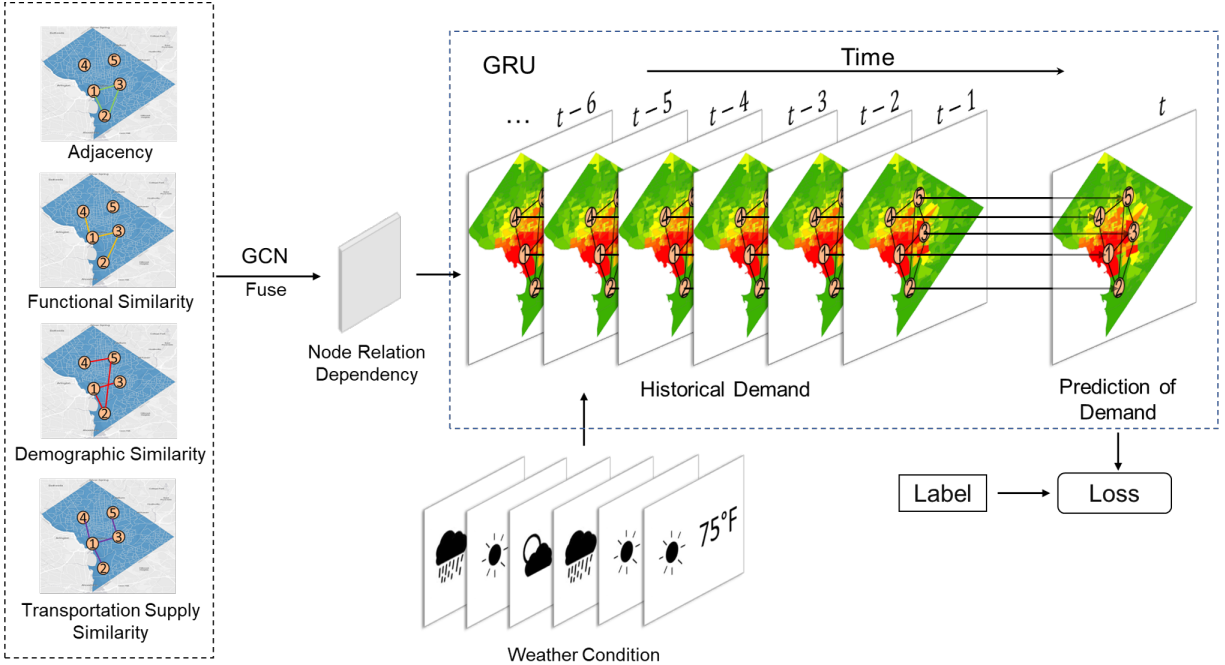


Figure 1: CA-STMGCN Model Framework

3.3. The GCN model

Extracting correlation dependency between different zones can enhance the performance of the dockless scooter-sharing demand prediction. For example, the neighborhood zones are more likely to have similar dockless scooter-sharing usage patterns, and that information can be used in demand prediction to improve the performance of the model. In previous studies, both convolutional neural network (CNN) and graph convolutional network (GCN) can be used to capture the spatial dependency (Geng et al., 2019; Yao et al., 2018; Zhao et al., 2019). However, the CNN can only be performed in Euclidean space, such as images and square grids, while GCN can handle graph-structured data (Zhao et al., 2019). Since the census block groups do not have a regular spatial structure but can be represented by a graph, we use GCN to capture node correlation dependency in this study.

Given an adjacency matrix A and the feature matrix X , GCN performs convolutional operation using a filter in the Fourier domain. The filter is applied on each node of the graph, thus capturing spatial dependency between the node and its adjacent nodes. The GCN model can be constructed by stacking multiple convolutional layers:

$$H^{l+1} = \sigma(\tilde{D}^{-\frac{1}{2}} \tilde{A} \tilde{D}^{-\frac{1}{2}} H^l W^l) \quad (2)$$

where H^l is the output of layer l and $H^0 = X$, $\tilde{A} = A + I$ is the adjacency matrix of the graph G with self-connections, I is the identity matrix, \tilde{D} is the diagonal node degree matrix of A , and W^l is a layer-specific trainable matrix. $\sigma(\cdot)$ denotes an activation function, such as the $ReLU(\cdot) = \max(0, \cdot)$ (Nair and Hinton, 2010). In this study, we use a 2-layer GCN

model introduced by Kipf and Welling (2016) to capture node correlation dependency. We first calculate $\hat{A} = \tilde{D}^{-\frac{1}{2}}\tilde{A}\tilde{D}^{-\frac{1}{2}}$ in a pre-processing step. The forward model then takes the form:

$$Z = f(X, A) = \text{softmax}(\hat{A} \text{ReLU}(\hat{A}XW^0) W^1) \quad (3)$$

where $W^0 \in \mathbb{R}^{C \times H}$ is the input-to-hidden weight matrix, C is the number of input channels (i.e., a C -dimensional feature vector for each node), H is the number of hidden units, $W^1 \in \mathbb{R}^{H \times F}$ is the hidden-to-output weight matrix, F is the number of filters, $Z \in \mathbb{R}^{N \times F}$ is the output convolved matrix, and N is the number of nodes. The softmax activation function, defined as $\text{softmax}(x_i) = \frac{1}{z} \exp(x_i)$ with $z = \sum_i \exp(x_i)$, is applied row-wise.

3.4. The GRU model

Among existing neural network models, RNN is the most widely used model to deal with sequence data. GRU (Cho et al., 2014) is a developed RNN model to process sequence data such as time series and speech signal data. Using the gating mechanism to memorize long-term information, GRU can well deal with the vanishing gradient problem that may happen in traditional RNN models. Compared with another widely used RNN model named LSTM (Hochreiter and Schmidhuber, 1997), GRU has fewer parameters thus is significantly faster to compute but still offers comparable performance in prediction (Chung et al., 2014). Therefore, we use GRU to model temporal dependency in this study.

GRU uses two gates, reset gate and update gate, to determine what information should be kept and passed to the output. The reset gate controls how much of the previous state information to remember, and the update gate determines how much of the past information needs to be passed to the new state. The structure of a GRU unit is presented in Figure 2.

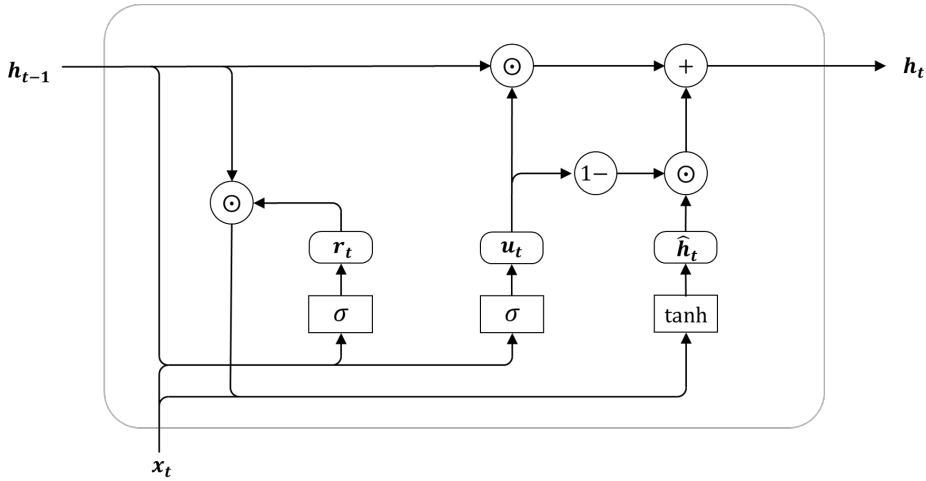


Figure 2: Structure of a GRU unit

The GRU unit takes the input of the current time step x_t and the hidden state of the previous time step h_{t-1} as inputs and outputs the new hidden state h_t . Given x_t and h_{t-1} ,

the reset gates r_t and the update gate u_t are calculated by fully-connected layers with an activation function σ . In the GRU model, sigmoid(Nwankpa et al., 2018) is used as the activation function. Mathematically, for a given time step t , the reset gates r_t and the update gate u_t are computed by:

$$r_t = \sigma(x_t W_{xr} + h_{t-1} W_{hr} + b_r) \quad (4)$$

$$u_t = \sigma(x_t W_{xu} + h_{t-1} W_{hu} + b_u) \quad (5)$$

where $W_{xr}, W_{hr}, W_{xu}, W_{hu}$ are weight parameters and b_r, b_u are biases.

Then we integrate the reset gate r_t with the hidden state of the previous time step h_{t-1} and the input of the current time step x_t to generate the candidate hidden state \hat{h}_t :

$$\hat{h}_t = \tanh(x_t W_{xh} + (r_t \odot h_{t-1}) W_{hh} + b_h) \quad (6)$$

where W_{xh}, W_{hh} are weight parameters, b_h is the bias, and \odot is the element-wise product operator.

Finally, we use the update gate u_t , the candidate hidden state \hat{h}_t , and the hidden state of the previous time step h_{t-1} to compute the current hidden state h_t . The new hidden state h_t is the output of the GRU unit and will be passed to the next time step. The current hidden state h_t is computed by:

$$h_t = u_t \odot h_{t-1} + (1 - u_t) \odot \hat{h}_t \quad (7)$$

3.5. Combining GCN and GRU

To capture the spatial dependency (i.e., node correlation dependency) and temporal dependency simultaneously, we integrate the GCN model and GRU model to generate a novel deep learning model named *Context-Aware Spatio-Temporal Multi-Graph Convolutional Network* (CA-STMGCN) to forecast the real-time dockless scooter-sharing demand. Let A denote the adjacency matrix of node correlation graph G and F^t denote the input feature matrix (i.e., dockless scooter-sharing demand and weather condition) at time t . We first use GCN to process the inputs A and F^t to extract spatial dependency matrix Z^t using Equation 3:

$$Z^t = f(F^t, A) = \text{softmax}(\hat{A} \text{ReLU}(\hat{A} F^t W^0) W^1) \quad (8)$$

Then we use the output matrix Z^t as the input of the GRU model. The calculation process in the GRU unit at time t becomes:

$$R_t = \sigma(Z^t W_{ZR} + H_{t-1} W_{HR} + b_R) \quad (9)$$

$$U_t = \sigma(Z^t W_{ZU} + H_{t-1} W_{HU} + b_U) \quad (10)$$

$$\hat{H}_t = \tanh(Z^t W_{ZH} + (R_t \odot H_{t-1}) W_{HH} + b_H) \quad (11)$$

$$H_t = U_t \odot H_{t-1} + (1 - U_t) \odot \hat{H}_t \quad (12)$$

where R_t is the reset gate, U_t is the update gate, H_{t-1} is the hidden state of the previous time step, \hat{H}_t is the candidate hidden state, H_t is the current hidden state, W_{ZR} , W_{HR} , W_{ZU} , W_{HU} , W_{ZH} , W_{HH} are weight parameters, and b_R , b_U , b_H are biases.

In summary, we first use the GCN model to capture node correlation dependency. Then we take the output of the GCN model as the input of the GRU model to capture the temporal dependency and eventually output the prediction. Therefore, the proposed CA-STMGCN model can capture both spatial and temporal dependency in the dockless scooter-sharing demand forecasting task.

3.6. Node correlation modeling

In this study, we use four graphs to respectively describe the spatial adjacency, functional similarity, demographic similarity, and transportation similarity of nodes, then input these graphs to the GCN model.

The spatial adjacency graph $G_{Adj} = (V, E_{Adj})$ is constructed by linking two geographically adjacent nodes i and j by an edge $e_{i,j} \in E_{Adj}$. Let A_{Adj} be the adjacency matrix of graph G_{Adj} , the element $a_{Adj}^{i,j} \in A_{Adj}$ is given by:

$$a_{Adj}^{i,j} = \begin{cases} 1, & \text{node } i \text{ and node } j \text{ are adjacent} \\ 0, & \text{otherwise} \end{cases} \quad (13)$$

The functional similarity graph $G_F = (V, E_F)$ is constructed by linking two nodes i and j that perform a similar function by an edge $e_{i,j} \in E_F$. The point of interest (POI) data is usually used to estimate the functional similarity between two nodes (Geng et al., 2019; Tang et al., 2021). Therefore, in this study, we calculate the POI similarity to quantify the functional similarity between two nodes and then determine whether the two nodes are functionally similar. The functional similarity graph is constructed using the same method in Tang et al. (2021). Let A_F denote the adjacency matrix of graph G_F , the element $a_F^{i,j} \in A_F$ is given by:

$$a_F^{i,j} = \begin{cases} 1, & sim(p_i, p_j) > d_F \\ 0, & \text{otherwise} \end{cases} \quad (14)$$

where $p_i \in \mathbb{R}^{1 \times n}$ and $p_j \in \mathbb{R}^{1 \times n}$ are the vectors of POI count of nodes i and j respectively, n is the number of POI categories, $sim(\cdot)$ is the calculation function of the Pearson coefficient, and d_F is the threshold parameter, which is set to 0.8 (Tang et al., 2021).

The demographic similarity graph is constructed by connecting two nodes i and j with similar demographic characteristics by an edge $e_{i,j} \in E_D$. The method we use to construct the demographic similarity graph is the same as the method to construct functional similarity graph. Let A_D denote the adjacency matrix of graph G_D , the element $a_D^{i,j} \in A_D$ is given by:

$$a_D^{i,j} = \begin{cases} 1, & \text{sim}(q_i, q_j) > d_D \\ 0, & \text{otherwise} \end{cases} \quad (15)$$

where $q_i \in \mathbb{R}^{1 \times m}$ and $q_j \in \mathbb{R}^{1 \times m}$ are the demographic feature vectors of nodes i and j respectively, m is the number of demographic features, $\text{sim}(\cdot)$ is the calculation function of the Pearson coefficient, and d_D is the threshold parameter, which is set to 0.8.

Similarly, the transportation supply similarity graph is constructed by connecting two nodes i and j with similar transportation supply characteristics by an edge $e_{i,j} \in E_T$. Let A_T denote the adjacency matrix of graph G_T , the element $a_T^{i,j} \in A_T$ is given by:

$$a_T^{i,j} = \begin{cases} 1, & \text{sim}(tr_i, tr_j) > d_T \\ 0, & \text{otherwise} \end{cases} \quad (16)$$

where $tr_i \in \mathbb{R}^{1 \times m}$ and $tr_j \in \mathbb{R}^{1 \times m}$ are the demographic feature vectors of nodes i and j respectively, m is the number of demographic features, $\text{sim}(\cdot)$ is the calculation function of the Pearson coefficient, and d_T is the threshold parameter, which is set to 0.8.

4. Case Study

In this section, we carried out a case study in Washington, D.C. to evaluate the proposed CA-STMGCN model. The performance of CA-STMGCN was then compared with the state-of-the-art benchmark models.

4.1. Data collection and description

The data we used include the real-time dockless scooter-sharing trip OD data, the weather condition data, the POI count data, and the demographic and transportation supply data in Washington, D.C. All the data was aggregated into the block group level. Table 1 presents the descriptive statistics of the input variables used in this study.

The real-time dockless scooter-sharing trip OD data was inferred from the General Bike-share Feed Specification (GBFS) data (NABSA, 2020) in Washington D.C. from June 19, 2019 to December 31, 2019. The data of four operators in Washington, D.C., including Bird, Lime, Lyft, and Spin, were collected. We collected the raw GBFS data using APIs provided by the vendors and then inferred the scooter trip origins and destinations using the algorithm developed by Xu et al. (2020). Note that we focused on trip generation (i.e., origin demand) prediction in this case study. We then aggregated the trip origins into the block group level and counted the trip origins with a 1-hour interval to obtain the hourly demand of each block group. The data from Jun 19, 2019 to Oct 22, 2019 was used as a training set, the data from October 23, 2019 to November 22, 2019 was used as a validation set, and the data from 23 November, 2019 to December 31 was used as a test set. Daily dockless scooter-sharing demand of different block groups in Washington, D.C. is shown in Figure 3.

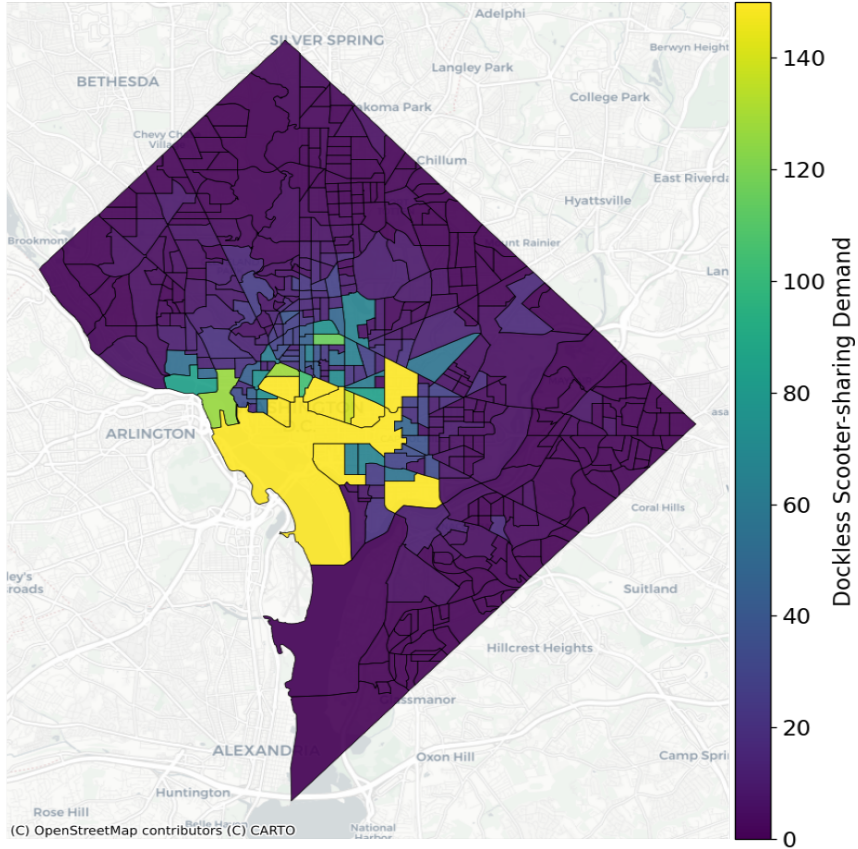


Figure 3: Daily dockless scooter-sharing demand of different block groups in Washington, D.C.

The weather condition data was collected from the *Global Historical Climatology Network (GHCN)*¹ database. The daily precipitation, average temperature, and average wind speed were used in the CA-STMGCN model.

We collected the POI location data from the *Open Data DC*² portal and the google map API ³. The collected POIs included education facilities, recreational facilities, government facilities, medical facilities, automobile service facilities, financial service facilities, tourism attractions, hotels, and grocery stores. Then we counted the POIs of each category in each block group based on the POI locations to generate the POI count data.

The demographic data used in this study included the population density, the proportion of the young population, the proportion of the white population, the female proportion, the proportion of population with bachelor's degree and above, the median household income, the proportion of households that own cars, and employment density. We also collected some transportation supply data including bike lane density, WalkScore (an index to evaluate the

¹<https://www.ncdc.noaa.gov/data-access/land-based-station-data/land-based-datasets/global-historical-climatology-network-ghcn>

²<https://opendata.dc.gov/>

³<https://developers.google.com/maps>

quality of walking environment), transit stop density, parking lot density, and road network density. These variables are selected because of their high correlations to the dockless scooter-sharing demand (Bai and Jiao, 2020; Merlin et al., 2021; Noland, 2021). We collected these kinds of data from various sources. The demographic data was collected from the *American Community Survey 2014-2018 5-year estimates* data. We used the *Walkscore.com* API to obtain the WalkScore of a block group centroid and applied geographic information system (GIS) techniques to calculate bike lane density, transit stop density, parking lot density, and road network density.

Table 1: Descriptive statistics of input variables

| Variables | Mean | Std. | Min | Max | Graph |
|---|--------|--------|--------|---------|----------------|
| Number of education facilities | 0.34 | 0.66 | 0 | 4 | |
| Number of recreational facilities | 0.33 | 0.75 | 0 | 4 | |
| Number of government facilities | 10.93 | 30.83 | 0 | 280 | |
| Number of medical facilities | 0.41 | 1.04 | 0 | 13 | Functional |
| Number of automobile service facilities | 0.09 | 0.36 | 0 | 3 | similarity |
| Number of financial service facilities | 0.47 | 2.18 | 0 | 35 | graph |
| Number of tourism attractions | 0.07 | 0.96 | 0 | 20 | |
| Number of hotels | 0.38 | 1.28 | 0 | 11 | |
| Number of grocery stores | 0.18 | 0.45 | 0 | 3 | |
| Population density (per sq. mile) | 21,029 | 16,424 | 24 | 115,859 | |
| Proportion of the young population | 32% | 16% | 1% | 100% | |
| Proportion of the white population | 41% | 33% | 0 | 100% | |
| Female proportion | 53% | 7% | 9% | 79% | Demographic |
| Proportion of population with BA's degree and above | 56% | 30% | 0 | 100% | similarity |
| Median household income (US dollar) | 96,519 | 55,202 | 12,229 | 250,001 | |
| Proportion of households own cars | 68% | 19% | 13% | 100% | |
| Employment density (per sq. mile) | 12,230 | 11,817 | 13 | 74,045 | |
| Bike lane density (mile per sq. mile) | 11.47 | 13.34 | 0 | 90.31 | Transportation |
| WalkScore | 73.47 | 21.84 | 4 | 99 | supply |
| Transit stop density (per sq. mile) | 571.08 | 408.86 | 25.43 | 3158.83 | similarity |
| Parking lot density (per sq. mile) | 142.48 | 106.43 | 0 | 589.81 | graph |
| Road network density (mile per sq. mile) | 53.24 | 20.28 | 10.19 | 134.29 | |
| Daily precipitation (inch) | 0.11 | 0.35 | 0 | 3.44 | |
| Average temperature (°F) | 65.76 | 16.55 | 29 | 91 | - |
| Average wind speed (m/s) | 7.88 | 2.75 | 2.91 | 17.67 | |

4.2. Model setting

After hyperparameter tuning, the learning rate of the CA-STMGCN model was set to 0.001. The batch size was set to 64. The number of hidden units was 32. The input time sequence length was 48. The model was trained using the Adam optimizer (Kingma and Ba, 2014), and the training epoch was 1000.

4.3. Models comparison

In this section, we compared the proposed CA-STMGCN model with several benchmark models. The details of these models are described as follows. Note that all the models were fine-tuned.

- **HA:** Historical Average is one of the most fundamental statistical models for time series prediction. HA predicts the demand in a specific time period by averaging historical observations.
- **ARIMA:** Auto-Regressive Integrated Moving Average is a statistical time series prediction model. ARIMA fits a parametric model based on historical observations to predict future demand. The order of ARIMA was set to (1,0,0) in the case study.
- **SVR:** Support Vector Regression (Smola and Schölkopf, 2004) is a machine learning model that uses the same principle as Support Vector Regression (SVM) but for regression problems. We used the Radial Basis Function kernel here. The cost was set to 1, and the gamma was set to 0.02.
- **GBDT:** Gradient Boosting Decision Tree (Friedman, 2001) is a tree-based ensemble machine learning model. In this case study, the number of trees was set to 2000, the maximum depth was set to 7, and the learning rate was set to 0.05.
- **RF:** Random Forest (Breiman, 2001) is another tree-based ensemble machine learning method. In this model, the number of trees was set to 110, and the number of features to consider when looking for the best split was set to 7.
- **MLP:** Multiple Layer Perceptron is a classical feedforward artificial neural network. In the case study, we used an MLP model with 100 neurons in the hidden layer. The activation function was ReLU. The learning rate was set to 0.001.
- **GRU:** Gated Recurrent Unit (Cho et al., 2014) is a widely used RNN model for time series modeling. The details of the GRU model are discussed in Section ???. The settings of this GRU model were consistent with the setting of the GRU model in the CA-STMGCN model.
- **LSTM:** Long Short-Term Memory (Hochreiter and Schmidhuber, 1997) is another widely used neural network based on the gating mechanism. In this model, the learning rate was 0.001, the batch size was 64, and the number of hidden units was 32.
- **T-GCN:** Temporal Graph Convolutional Network (Zhao et al., 2019) is a spatiotemporal graph convolutional neural network that captures spatial and temporal dependency simultaneously. The spatial adjacency graph G_{Adj} was used as the input of the GCN model in the T-GCN model. The settings of the T-GCN model were consistent with the settings of the CA-STMGCN model.

- **MC-STGCN**: The Multi-Community Spatio-Temporal Graph Convolutional Network (Tang et al., 2021) is an advanced spatiotemporal graph convolutional neural network for passenger demand prediction. The model was trained using Adam optimizer with learning rate of 0.001. The batch size was set to 64. The number of hidden units was set to 32.

We evaluated the performance of the models using two metrics: RMSE (Root Mean Square Error) and MAE (Mean Absolute Error). The calculation of the two metrics is:

$$RMSE = \sqrt{\frac{1}{N} \sum_{k=1}^N (\hat{y}_k - y_k)^2} \quad (17)$$

$$MAE = \frac{1}{N} \sum_{k=1}^N |\hat{y}_k - y_k| \quad (18)$$

Table 2: Performance of the CA-STMGCN model and the benchmark models

| Methods | MAE | RMSE |
|-----------|---------------|---------------|
| HA | 0.3408 | 0.7001 |
| ARIMA | 0.5591 | 0.9999 |
| SVR | 0.2961 | 0.6964 |
| GBDT | 0.3579 | 0.6832 |
| RF | 0.3714 | 0.7160 |
| MLP | 0.3542 | 0.6867 |
| GRU | 0.2079 | 0.5286 |
| LSTM | 0.2269 | 0.5403 |
| T-GCN | 0.1308 | 0.3543 |
| MC-STGCN | 0.1121 | 0.3492 |
| CA-STMGCN | 0.0889 | 0.2285 |

The performances of these models are shown in Table 2. We can see that the CA-STMGCN model outperformed all the benchmark models. The RNN models (i.e., GRU and LSTM) had better prediction performance than the statistical models (i.e., HA and ARIMA), the machine learning models (i.e., SVR, GBDT, and RF), and the classical neural network model (i.e., MLP), which demonstrated their effectiveness in time series modeling tasks. Among the two RNN models, GRU slightly outperformed LSTM. The spatiotemporal neural network models (i.e., T-GCN, MC-STGCN, CA-STMGCN) significantly outperformed the RNN models, which can only capture temporal dependency. This result indicated that there exist strong spatial correlations among nodes, and the GCN components with well-designed

graphs can well capture these correlations. The multi-graph model (i.e., CA-STMGCN and MC_STGCN) had better performance than T-GCN, which took single-graph input. This implied that the more comprehensive spatial information provided by multiple graphs with a well-tuned fusing scheme can improve the model performance. The performance of CA-STMGCN model was better than MC_STGCN, which did not take weather conditions and demographic and transportation supply factors into account. This result indicated that considering more variables that are correlated to demand can enhance dockless scooter-sharing demand forecasting.

4.4. *Ablation study*

We then conducted a ablation study for the proposed model. The ablation study examines the performance of the model by removing certain components to see the contribution of the removed components (Meyes et al., 2019). In this ablation study, we generated five models by removing spatial adjacency graph, functional similarity graph, demographic similarity graph, transportation supply similarity graph, or weather information respectively.

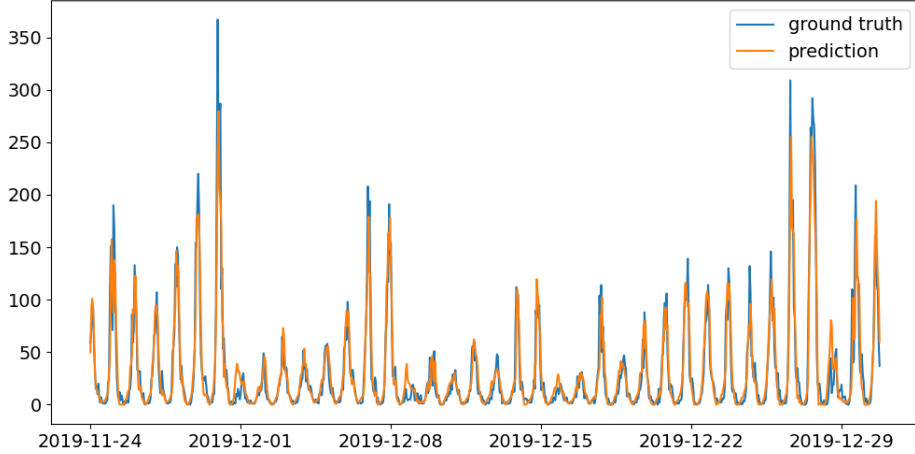
The performance of the five ablated models is presented in Table 3. The results suggested that the weather information, the spatial adjacency graph, the functional similarity graph, and the demographic and built environment contributed to the prediction accuracy, and the weather information contributed most. According to the results, the prediction error increased a lot when removing the weather information (MAE increased 30%, and RMSE increased 48%). This result indicates that the weather information can greatly improve the model performance. It is reasonable because the use of dockless scooter-sharing is sensitive to the weather condition. For example, the use of dockless scooter-sharing will significantly decrease when it is cold and rainy (Noland, 2021). Additionally, a relatively small increase of prediction error (6% for MAE and 2% for RMSE) occurred when we removed the spatial adjacency graph. This indicates that although the spatial adjacency graph improved the model performance, the contribution of this component was limited. The prediction accuracy of the model also decreased when we removed the functional similarity graph (6% for MAE and 9% for RMSE), the demographic similarity graph (10% for MAE and 3% for RMSE), and the transportation supply similarity graph (8% for MAE and 12% for RMSE), which suggests that these components can enhance the model performance. It is worth noting that the influence of the spatial adjacency graph and the demographic similarity graph on RMSE is small, which indicates that the effect of these two graphs on the model’s ability to reduce large prediction errors is limited.

Table 3: Results of ablation study

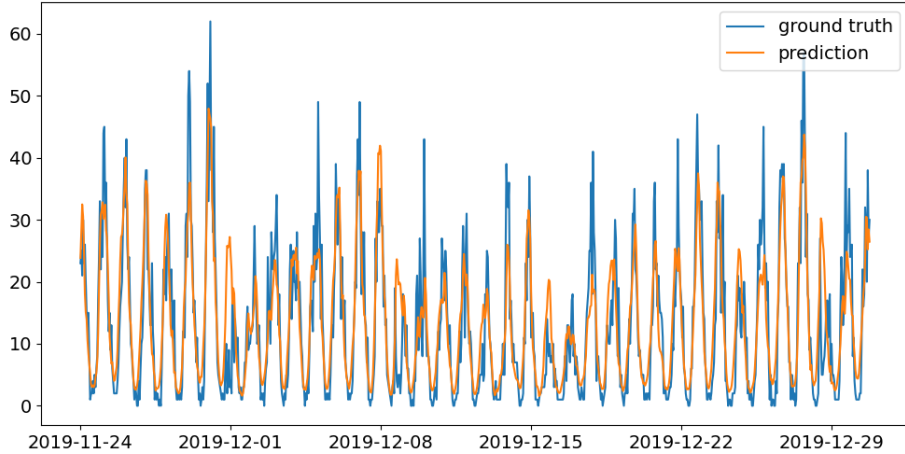
| Methods | MAE | RMSE |
|--|---------------|---------------|
| CA-STMGCN | 0.0889 | 0.2285 |
| w/o Spatial adjacency graph | 0.0944 | 0.2335 |
| w/o Functional similarity graph | 0.0943 | 0.2494 |
| w/o Demographic similarity graph | 0.0981 | 0.2345 |
| w/o Transportation supply similarity graph | 0.0963 | 0.2569 |
| w/o Weather information | 0.1157 | 0.3376 |

4.5. Prediction results

We further compared the prediction of the CA-STMGCN model and the observed demand using the data in the test set (i.e., the data from November 23, 2019 to December 31, 2019). We selected two regions with high demand variance and different maximum demand volume. The results are presented in Figure 4. As we can see, the temporal distributions of the dockless scooter-sharing demand in the two regions had different demand intensity. The temporal distributions of the observed demand and the model prediction are largely similar. Although the model sometimes cannot fully capture extreme values, the model prediction can effectively follow the temporal fluctuation of observed data in different regions and different time periods. It is worth noting that there were obvious peaks of demand in these figures. These peaks usually occurred over the weekends, and the proposed model performed well in predicting these peak demands.



(a) Region 1



(b) Region 2

Figure 4: Comparison of CA-STMGCN model prediction and ground truth demand

5. Discussion and Conclusion

In this study, we propose a novel deep learning model *Context-Aware Spatio-Temporal Multi-Graph Convolutional Network* (CA-STMGCN) for real-time dockless scooter-sharing demand forecasting. The proposed CA-STMGCN integrates zonal context (i.e., functionality, demographic characteristics, and transportation supply) and weather conditions to account for spatiotemporal demand prediction. We construct four graphs (i.e., spatial adjacency graph, functional similarity graph, demographic similarity graph, and transportation supply graph) to represent the spatial correlations between block groups. Then we use a

GCN model to extract spatial dependency from the graphs and use a GRU model to take the historical demand data and weather condition data to extract temporal dependency. A fully connected neural network layer is used to generate the final prediction. The proposed model is evaluated using the real-world dockless scooter-sharing demand data in Washington, D.C. and compared with the state-of-the-art benchmark models. The results show that the proposed model outperforms all the selected benchmark models benefited from its ability to consider weather conditions and capture comprehensive spatial dependency. According to the ablation study, the most important model component is the weather information, which is omitted by most of the existing spatiotemporal demand prediction studies. The proposed model can help the operators develop optimal vehicle charging and rebalancing schemes and guide cities to regulate the dockless scooter-sharing system.

Although the proposed CA-STMGCN model has achieved high prediction accuracy, several limitations still require future work. Firstly, more external features such as emergency/special events and holidays can be incorporated to enhance the prediction performance. For example, the dockless scooter-sharing usage patterns can be unique on holidays such as Christmas and the New Year's Day, because more tourism trips may take place on holidays. Secondly, we use daily weather condition data to forecast the hourly dockless scooter-sharing demand in this study. Weather condition data with a smaller time interval (e.g., hourly) may be collected and used to reflect more precise weather conditions in the CA-STMGCN and potentially achieve a better predictive performance in future work.

References

M. H. Amini, A. Kargarian, and O. Karabasoglu. Arima-based decoupled time series forecasting of electric vehicle charging demand for stochastic power system operation. *Electric Power Systems Research*, 140: 378–390, 2016.

H. I. Ashqar, M. Elhenawy, H. A. Rakha, M. Almannaa, and L. House. Network and station-level bike-sharing system prediction: a san francisco bay area case study. *Journal of Intelligent Transportation Systems*, pages 1–11, 2021.

S. Bai and J. Jiao. Dockless e-scooter usage patterns and urban built environments: A comparison study of austin, tx, and minneapolis, mn. *Travel behaviour and society*, 20:264–272, 2020.

L. Breiman. Random forests. *Machine learning*, 45(1):5–32, 2001.

Z. Cao, X. Zhang, K. Chua, H. Yu, and J. Zhao. E-scooter sharing to serve short-distance transit trips: A singapore case. *Transportation research part A: policy and practice*, 147:177–196, 2021.

O. Caspi, M. J. Smart, and R. B. Noland. Spatial associations of dockless shared e-scooter usage. *Transportation Research Part D: Transport and Environment*, 86:102396, 2020.

P.-C. Chen, H.-Y. Hsieh, K.-W. Su, X. K. Sigalingging, Y.-R. Chen, and J.-S. Leu. Predicting station level demand in a bike-sharing system using recurrent neural networks. *IET Intelligent Transport Systems*, 14 (6):554–561, 2020.

K. Cho, B. Van Merriënboer, D. Bahdanau, and Y. Bengio. On the properties of neural machine translation: Encoder-decoder approaches. *arXiv preprint arXiv:1409.1259*, 2014.

Z. Christoforou, C. Gioldasis, A. de Bortoli, and R. Seidowsky. Who is using e-scooters and how? evidence from paris. *Transportation research part D: transport and environment*, 92:102708, 2021.

J. Chung, C. Gulcehre, K. Cho, and Y. Bengio. Empirical evaluation of gated recurrent neural networks on sequence modeling. *arXiv preprint arXiv:1412.3555*, 2014.

J. H. Friedman. Greedy function approximation: a gradient boosting machine. *Annals of statistics*, pages 1189–1232, 2001.

X. Geng, Y. Li, L. Wang, L. Zhang, Q. Yang, J. Ye, and Y. Liu. Spatiotemporal multi-graph convolution network for ride-hailing demand forecasting. In *Proceedings of the AAAI conference on artificial intelligence*, volume 33, pages 3656–3663, 2019.

S. Hochreiter and J. Schmidhuber. Long short-term memory. *Neural computation*, 9(8):1735–1780, 1997.

A. Hosseinzadeh, M. Algomaiah, R. Kluger, and Z. Li. E-scooters and sustainability: Investigating the relationship between the density of e-scooter trips and characteristics of sustainable urban development. *Sustainable cities and society*, 66:102624, 2021.

J. Ke, X. Qin, H. Yang, Z. Zheng, Z. Zhu, and J. Ye. Predicting origin-destination ride-sourcing demand with a spatio-temporal encoder-decoder residual multi-graph convolutional network. *Transportation Research Part C: Emerging Technologies*, 122:102858, 2021.

T. S. Kim, W. K. Lee, and S. Y. Sohn. Graph convolutional network approach applied to predict hourly bike-sharing demands considering spatial, temporal, and global effects. *PLoS one*, 14(9):e0220782, 2019.

D. P. Kingma and J. Ba. Adam: A method for stochastic optimization. *arXiv preprint arXiv:1412.6980*, 2014.

T. N. Kipf and M. Welling. Semi-supervised classification with graph convolutional networks. *arXiv preprint arXiv:1609.02907*, 2016.

B. Laa and U. Leth. Survey of e-scooter users in vienna: Who they are and how they ride. *Journal of transport geography*, 89:102874, 2020.

H. Lee, K. Baek, J.-H. Chung, and J. Kim. Factors affecting heterogeneity in willingness to use e-scooter sharing services. *Transportation Research Part D: Transport and Environment*, 92:102751, 2021.

Y. Li, Z. Zhu, D. Kong, M. Xu, and Y. Zhao. Learning heterogeneous spatial-temporal representation for bike-sharing demand prediction. In *Proceedings of the AAAI Conference on Artificial Intelligence*, volume 33, pages 1004–1011, 2019.

L. Lin, Z. He, and S. Peeta. Predicting station-level hourly demand in a large-scale bike-sharing network: A graph convolutional neural network approach. *Transportation Research Part C: Emerging Technologies*, 97:258–276, 2018.

L. Liu, Z. Qiu, G. Li, Q. Wang, W. Ouyang, and L. Lin. Contextualized spatial-temporal network for taxi origin-destination demand prediction. *IEEE Transactions on Intelligent Transportation Systems*, 20(10):3875–3887, 2019.

J. K. Mathew, M. Liu, and D. M. Bullock. Impact of weather on shared electric scooter utilization. In *2019 IEEE Intelligent Transportation Systems Conference (ITSC)*, pages 4512–4516. IEEE, 2019.

G. McKenzie. Spatiotemporal comparative analysis of scooter-share and bike-share usage patterns in washington, dc. *Journal of transport geography*, 78:19–28, 2019.

L. A. Merlin, X. Yan, Y. Xu, and X. Zhao. A segment-level model of shared, electric scooter origins and destinations. *Transportation Research Part D: Transport and Environment*, 92:102709, 2021.

R. Meyers, M. Lu, C. W. de Puiseau, and T. Meisen. Ablation studies in artificial neural networks. *arXiv preprint arXiv:1901.08644*, 2019.

R. Mitra and P. M. Hess. Who are the potential users of shared e-scooters? an examination of socio-demographic, attitudinal and environmental factors. *Travel behaviour and society*, 23:100–107, 2021.

NABSA. General bikeshare feed specification. <https://github.com/NABSA/gbfs>, 2020.

NACTO. Shared micromobility in the u.s.: 2018. *New York, NY*, 2019.

V. Nair and G. E. Hinton. Rectified linear units improve restricted boltzmann machines. In *Icml*, 2010.

R. B. Noland. Scootin'in the rain: Does weather affect micromobility? *Transportation Research Part A: Policy and Practice*, 149:114–123, 2021.

C. Nwankpa, W. Ijomah, A. Gachagan, and S. Marshall. Activation functions: Comparison of trends in practice and research for deep learning. *arXiv preprint arXiv:1811.03378*, 2018.

Y. Pan, R. C. Zheng, J. Zhang, and X. Yao. Predicting bike sharing demand using recurrent neural networks. *Procedia computer science*, 147:562–566, 2019.

R. L. Sanders, M. Braniion-Calles, and T. A. Nelson. To scooter or not to scooter: Findings from a recent survey about the benefits and barriers of using e-scooters for riders and non-riders. *Transportation Research Part A: Policy and Practice*, 139:217–227, 2020.

J. Schuijbroek, R. C. Hampshire, and W.-J. Van Hoeve. Inventory rebalancing and vehicle routing in bike sharing systems. *European Journal of Operational Research*, 257(3):992–1004, 2017.

B. L. Smith, B. M. Williams, and R. K. Oswald. Comparison of parametric and nonparametric models for traffic flow forecasting. *Transportation Research Part C: Emerging Technologies*, 10(4):303–321, 2002.

A. J. Smola and B. Schölkopf. A tutorial on support vector regression. *Statistics and computing*, 14(3):199–222, 2004.

J. Tang, J. Liang, F. Liu, J. Hao, and Y. Wang. Multi-community passenger demand prediction at region level based on spatio-temporal graph convolutional network. *Transportation Research Part C: Emerging Technologies*, 124:102951, 2021.

J. Xu, R. Rahmatizadeh, L. Bölöni, and D. Turgut. Real-time prediction of taxi demand using recurrent neural networks. *IEEE Transactions on Intelligent Transportation Systems*, 19(8):2572–2581, 2017.

Y. Xu, X. Yan, V. P. Sisiopiku, L. A. Merlin, F. Xing, and X. Zhao. Micromobility trip origin and destination inference using general bikeshare feed specification (gbfs) data. *arXiv preprint arXiv:2010.12006*, 2020.

Y. Xu, X. Yan, X. Liu, and X. Zhao. Identifying key factors associated with ridesplitting adoption rate and modeling their nonlinear relationships. *Transportation Research Part A: Policy and Practice*, 144:170–188, 2021.

X. Yan, X. Liu, and X. Zhao. Using machine learning for direct demand modeling of ridesourcing services in chicago. *Journal of Transport Geography*, 83:102661, 2020.

H. Yao, F. Wu, J. Ke, X. Tang, Y. Jia, S. Lu, P. Gong, J. Ye, and Z. Li. Deep multi-view spatial-temporal network for taxi demand prediction. In *Proceedings of the AAAI Conference on Artificial Intelligence*, volume 32, 2018.

H. Younes, Z. Zou, J. Wu, and G. Baiocchi. Comparing the temporal determinants of dockless scooter-share and station-based bike-share in washington, dc. *Transportation Research Part A: Policy and Practice*, 134:308–320, 2020.

L. Zhao, Y. Song, C. Zhang, Y. Liu, P. Wang, T. Lin, M. Deng, and H. Li. T-gcn: A temporal graph convolutional network for traffic prediction. *IEEE Transactions on Intelligent Transportation Systems*, 21(9):3848–3858, 2019.

R. Zhu, X. Zhang, D. Kondor, P. Santi, and C. Ratti. Understanding spatio-temporal heterogeneity of bike-sharing and scooter-sharing mobility. *Computers, Environment and Urban Systems*, 81:101483, 2020.